

Vacuum-Deposited Transparent Organic Photovoltaics for Efficiently Harvesting Selective Ultraviolet and Near-Infrared Solar Energy

by Meng-zhen Li

Submission date: 17-Apr-2023 03:44AM (UTC+0700)

Submission ID: 2066167793

File name: otovoltaics_for_Efficiently_Harvesting_Selective_Ultraviolet.pdf (1.14M)

Word count: 10306

Character count: 49279

Vacuum-Deposited Transparent Organic Photovoltaics for Efficiently Harvesting Selective Ultraviolet and Near-Infrared Solar Energy

Meng-Zhen Li, Chih-Chien Lee, Sajal Biring, I-Sheng Hsu, Dian Luo, Richie Estrada, Yi-Shiuan Wu, Chun-Chen Yang, and Shun-Wei Liu*

Highly transparent photovoltaics (TPVs) integrated to a battery with small capacity can efficiently drive low-powered internet of things (IoT) devices such as the receivers, sensors, actuators, etc. Such see-through solar technology not only provides an opportunity to convert ambient light (sunlight or indoor lighting) to electricity but also demonstrates a concept of self-sustainable power. In this work, a selective ultraviolet/near-infrared bulk-heterojunction active layer, i.e., chloroaluminum phthalocyanine (ClAlPc) as donor and C₆₀ as acceptor with a Cu:Ag/WO₃ transparent electrode to visible lights are combined for achieving the vacuum-deposited TPVs with a power conversion efficiency of 1.34%, average visible transmission of 77.45%, and color rendering index of 91.9. Moreover, a TPV module with a working area of 1.5 cm² is able to charge a 0.58 mAh LiFePO₄(LFP)//Li battery fully within one hour under 100 mW cm⁻² (≈1 sun) illumination. The TPV module can drive an exciplex organic light-emitting diode with the electroluminescence >180 cd m⁻² at low illumination intensity of <5 mW cm⁻². Overall, this work presents a significant step forward in the development of TPV technology towards integrating a display and storage battery, which could be successfully applied in wearable electronics requiring invisible and sustainable solar power.


1. Introduction

Highly transparent photovoltaics (TPVs) are one of the most critical technologies for imposing a building aesthetics, because the TPVs can efficiently harvest selective ultraviolet (UV) and near-infrared (NIR) solar energy to power a low-consumption electronics.^[1–3] Polymers,^[4–7] small molecules,^[8] organic dye and dye-sensitized,^[9–12] halide perovskite,^[13,14] and lead halide^[15,16] have been studied extensively as active layers for TPVs to demonstrate wavelength-selective TPVs with an average visible transmission (AVT) of >50% and a color rendering index (CRI) of >80. Regarding the concept of life aesthetics for humans, the type of wavelength-selective TPVs is a smart solution for integration with the buildings, wearable electronics, vehicles, and greenhouses.^[1–3] This implies that the AVT value of TPV needs to exceed 75% or similar to glass, which can satisfy the customer's application-specific design to develop novel and transparent products.

M.-Z. Li, Prof. S. Biring, I.-S. Hsu, D. Luo, Prof. S.-W. Liu
Organic Electronics Research Center
Ming Chi University of Technology
New Taipei City 24301, Taiwan
E-mail: swliu@mail.mcut.edu.tw

M.-Z. Li, Prof. C.-C. Lee, R. Estrada
Department of Electronic Engineering
National Taiwan University of Science and Technology
Taipei 10617, Taiwan

Prof. S. Biring, Prof. S.-W. Liu
Department of Electronic Engineering
Ming Chi University of Technology
New Taipei City 24301, Taiwan

 The ORCID identification number(s) for the author(s) of this article can be found under <https://doi.org/10.1002/solr.202000564>.

© 2020 The Authors. Solar RRL published by Wiley-VCH GmbH. This is an open access article under the terms of the Creative Commons Attribution-NonCommercial-NoDerivs License, which permits use and distribution in any medium, provided the original work is properly cited, the use is non-commercial and no modifications or adaptations are made.

DOI: 10.1002/solr.202000564

D. Luo
Institute of Lighting and Energy Photonics
College of Photonics
National Chiao Tung University
Tainan 71150, Taiwan

Dr. Y.-S. Wu, Prof. C.-C. Yang
Battery Research Center of Green Energy
Ming Chi University of Technology
New Taipei City 24301, Taiwan

Prof. C.-C. Yang
Department of Chemical Engineering
Ming Chi University of Technology
New Taipei City 24301, Taiwan

Prof. C.-C. Yang
Department of Chemical and Materials Engineering
Chang Gung University
Taoyuan City 33302, Taiwan

For example, Lunt and Bulovic have demonstrated a NIR selective transparent planar organic photovoltaics (PVs) with AVT > 55% and the power conversion efficiency (PCE) > 1.7%.^[8] This work opened a new vision that the functional materials or structures can offer a peak absorption in the UV and NIR or specific absorption range, resulting in an efficient TPV with high AVT. Later on, the research team by Lunt also demonstrated another approach with the NIR harvesting transparent luminescent solar concentrators (LSCs).^[17,18] The transparent LSCs exhibited nontinted transparency > 86% in the visible-light with edge-mounted Si PV to achieve the PCE > 0.4%. Therefore, TPV with high transparency has great potential in unique solar energy applications, which improves the device performance.

Considering the previous work of wavelength-selective TPVs, only a few studies can demonstrate the TPV with AVT > 70% and PCE > 1%. This is because the PCE of TPV strongly depends on the value of AVT. While AVT exceeds 60%, the device performance drops dramatically, especially the TPV's short-circuit current. As a consequence, to improve the critical parameters of TPVs, i.e., AVT and PCE, increasing the absorption range in the UV or NIR region and allowing the absorption in the visible-light region are fundamental design rules. More recently, tuning halide perovskite's bandgap to selectively harvest near-UV light (≈ 410 and 440 nm) offered the state-of-the-art AVT value > 70% and CRI > 90.^[13–16] Although such an approach of tunable bandgap recommends halide perovskite as a potential candidate for TPV applications, the overall device performance is not capable of providing sufficient energy to drive the low-power electronics because of the low PCE of $\approx 0.52\%$. Therefore, a new method for developing the TPV with high PCE, AVT, and CRI is still in need. In 2018, Liu et al. reported a lead halide UV-harvesting TPV with high stability, which achieved an AVT > 70% with PCE > 1%.^[13] This work successfully solved the problems related to optical losses, complex coating processes, etc. In addition, the lead halide bilayer showed a high color rendering index (CRI), because PbI₂/C₆₀ mainly absorbs the wavelength less than 500 nm satisfying the concept of UV-selective TPV. As the lead halide TPV has ultrahigh transparency in the visible light, we believe that such technology shows exceptional promise for large-scale solar energy harvesting to absorb the sunlight from outdoor or very weak indoor lighting from the interior of buildings. Even a cover glass with a small-scale TPV can possibly drive watch's LCDs or microelectronics in the future.

In this work, we report a vacuum-deposited highly transparent TPV using a mixed active layer of chloroaluminum phthalocyanine (ClAlPc) as donor and C₆₀ as acceptor, which achieved the PCE > 1.3% with an AVT of 77.45% and CRI of 91.9. The proposed device configuration of the TPV provides a useful method to develop transparent solar glass where high transmittance in visible lights is an important parameter. Therefore, these results not only demonstrate the vacuum-deposited TPV with the highest AVT's value but also provide a route to fabricate transparent electrode consisting of Cu:Ag metal alloy and capping layer of WO₃. It is worthwhile to mention that the ultrathin ClAlPc: C₆₀ active layer shows UV/NIR absorption ability, which is advantageous for developing a novel light-sensing or absorption electronics, such as NIR sensitive organic photovoltaics (OPVs),^[19] semi-TPVs,^[8] multitandem OPVs,^[20] wide-absorption

range organic photodetector,^[21] organic upconversion devices,^[22] etc. On the other hand, to further investigate the optical effect on our proposed TPV, we have used optical modeling to optimize each layer, i.e., organic active layer and transparent electrode for higher transmittance and lower reflection of lights in the devices. In addition, a TPV module designed with the optimal device structure successfully charges a 0.58 mAh battery fully within 1 h under 1 sun illuminance. The solar module can even drive an exciplex organic light-emitting diode (OLED) with emission intensity > 180 cd m⁻² under low-level sunlight of 5 mW cm⁻² (≈ 0.05 sun). To the best of our knowledge, an invisible sustainable solar power for charging a battery or driving an OLED efficiently is demonstrated successfully for the first time.

2. Results and Discussion

2.1. The Optical Property of Ultrathin Cu:Ag Electrode and WO₃ Capping Layer

Highly transparent efficient electrodes are indispensable for novel electronic applications, such as transparent displays,^[23] augmented reality glasses,^[24] wearable sensors,^[25–27] semitransparent solar windows,^[28–30] etc.^[31] Among these transparent anode or cathode electrodes, the electrodes with the multilayered structure, i.e., buffer layer/thin metal/buffer layer, provide efficient charge injection, high transparency, and excellent mechanical flexibility as compared to the standard transparent conductive oxides.^[32] But, to achieve high AVT and PCE of a TPV, the transparent electrode should possess several particular optoelectrical properties. For example, a transparent multilayered electrode needs to offer a high transmittance value in the range of 450–650 nm and reflect only the NIR/UV light. Accordingly, the ultrathin Ag (< 15 nm) with a capping layer is often used to form the vacuum-deposited transparent electrode having the transmittance (T%) > 75% in the range of the visible light, which is much better than that of neat thin Ag (T% < 60% at 550 nm).^[33]

As the insertion of the capping layer can further improve the transmission property of the thin metal, the tris(8-hydroxyquinoline)aluminum (Alq₃) or molybdenum oxide (MoO₃) acts as an optical buffer layer to enhance the transparency of TPVs in visible lights.^[14–16] In 2013, a multilayered Ag/Alq₃ electrode was proposed that could reflect NIR light to achieve an efficient electron collection efficiency of semitransparent OPVs with cyanine dye.^[9] In addition, this transparent electrode was also used to harvest UV lights resulting in TPV with AVT of 73% and a CRI over 93. Following the similar optical engineering concept, Ag/MoO₃ electrode has been adopted widely in transparent organic electronics. Several experimental works have demonstrated enhanced transparency of the devices by depositing an optical thin film with a high refractive index on the thin-Ag layer.^[24] For example, vacuum-deposited WO₃/Ag/WO₃,^[33] TiO₂/Ag/AZO,^[34] NiO/Ag/NiO,^[35] graded Ag/NPB,^[36] and MoO₃/Ag/WO₃^[37] multilayered electrodes showed high transmission of > 80% and low sheet resistance of < 10 Ω sq⁻¹.

More recently, Hanmandlu et al. reported bifacial perovskite solar cells featuring a semitransparent electrode, where BCP/Ag/MoO₃ cathode not only shows the transmission value of $\approx 65\%$ at 550 nm but can also reflect the UV/NIR light effectively.^[14] This

approach illustrates that the transmission value of the electrode limits the potential of TPVs. Standard TPV's (polymer, small molecule, lead halide, or perovskite-based) AVT value still cannot exceed 75% due to the electrodes without high transmission property in the visible light. Therefore, proper optimization of these multilayered electrodes to achieve high AVT and UV/NIR reflection is crucial for improving the performance of TPVs.

In previous studies, several works demonstrated that surface morphology is an instrumental parameter to determine the optical property of ultrathin Ag film.^[38–40] One of the simplest and feasible methods to control the nanostructure or surface morphology of the thin metal film is to inject inhomogeneous metal seeds during the growth process. For example, Li et al. reported that 8 nm-thick Cu:Ag film grown by cosputtering showed the AVT of 72%, which is much higher than that of pure Ag film.^[41] The experimental result indicated that Cu atoms acted as the nucleation sites assisting in the continuous growth of a uniform ultrathin Ag film by eradicating the aggregation effect, resulting in the enhancement of the optical property. In this work, we have fabricated Cu:Ag film ($\approx 2\%$ Cu in Ag) combined with the capping layer of WO_3 by thermal evaporation technique to tune its optical property in the visible light. As a consequence, we find that the Cu doping induces ultrathin Ag film with highly smooth surface morphology, i.e., root mean square (RMS) roughness of ≈ 0.5 nm (Figure 1a), compared with that of the thin Ag film (RMS = 1.98 nm; Figure 1b). Note that the RMS value for Cu:Ag film prepared by thermal evaporation is slightly smoother than previous work using the cosputtering technique (RMS = 0.7 nm for an 8 nm Cu:Ag film).^[36] In general, Ag film tends to grow as following the Volmer–Weber mode,^[42–44] which forms a rough surface on the 8 nm-thick Ag film (Figure 1c). Thus, such a nanorugged profile of thin metal film may cause a significant scattering loss on Ag's surface, which is detrimental to integrate with the optical buffer for efficient UV/NIR reflection and higher transmission of visible light. As it is obvious from Figure 2a that such a rough surface profile of the thin Ag film exhibits a constant reflection of $\approx 15\%$ in the range from 450 to 750 nm. In contrast, Cu:Ag film with the ultrasmooth surface (Figure 1) sharply reduces the localized plasmon resonance effect and therefore alters the reflection profile compared with that of pure Ag film in the visible light.^[45–47] Here, we have varied the concentration of Cu into Ag to optimize the reflection profile of the Cu:Ag (x ratio)/ WO_3 (30 nm)

electrode, as shown in Figure 2b. Such an electrode not only allows the light from the 450 to 650 nm to pass through but also partially reflects the UV/NIR light to fit the absorption spectrum of the ClAlPC: C_{60} active layer. As a result, the peak reflection value at 550 nm is almost two times lower than that of the Ag/ WO_3 . Moreover, a strong resonant optical cavity formed between the indium tin oxide (ITO) and Cu:Ag/ WO_3 might increase the light harvesting close to the proposed photoactive absorber, resulting in the enhancement of the device performance of TPVs. From the reflection results, we found that different concentrations of Cu into Ag positively affects the optical property because of the preferred nucleation sites to induce lateral Ag film growth. Therefore, the appropriate mixing of Cu in Ag is expected to provide a high transmission profile in the region of the photopic spectral response. To confirm our hypothesis, we studied the transmission spectra (Figure 2c) of the electrodes with different ratios of Cu:Ag (8 nm; mixing ratio of 1:50, 1:30, and 1:10)/ WO_3 (30 nm). The optimized transparent Cu:Ag electrode with 1:50 exhibits high reflection in the NIR zone and a high AVT value of $\approx 78.62\%$ outperforming Ag/ WO_3 (AVT = 46.88%) and similar to ITO (AVT = 89%) electrodes (see Figure S1, Supporting Information). It is noteworthy that capping layer of WO_3 can also preserve the surface morphology of Cu:Ag or Ag in the ambient under high-temperature aging (Figure S2, Supporting Information). This result is even comparable with that of the highly transparent $\text{WO}_3/\text{Ag}/\text{WO}_3$ multilayered electrodes.^[33] On the other hand, the Cu:Ag film shows ultrasmooth surface morphology as revealed in atomic force microscope (AFM) topography (Figure 1), which is favorable to achieve high electrical conductivity. Our proposed Cu:Ag electrode's sheet resistance is $10.5 \Omega \text{sq}^{-1}$ compared with $12 \Omega \text{sq}^{-1}$ for 8 nm Ag. Therefore, the experimental result implies that our proposed ultrathin transparent electrode with a superior electrical conduction characteristic can replace the standard ITO electrode or thin metal in TPV applications.

2.2. Vacuum-Deposited Wavelength-Selective UV/NIR Organic Photovoltaics with Opaque and Transparent Electrodes

The recent application of the TPVs is in the building-integrated window without requiring an additional kit to harvest energy efficiently. But, for the high-end mobile electronic applications of TPVs, the value of AVT requires to be even $>75\%$ and

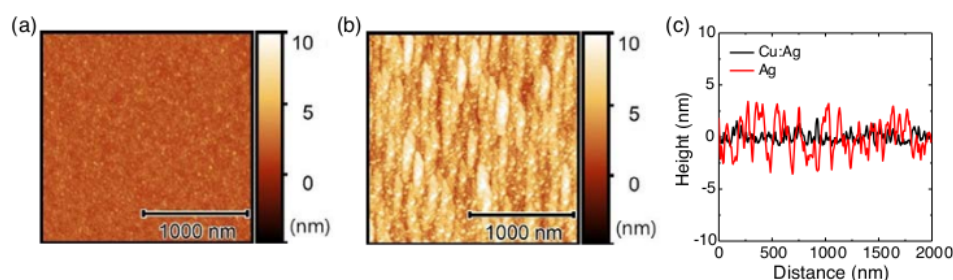


Figure 1. c) Representative surface morphologies by AFM for a) 8 nm Cu:Ag (1:50) and b) 8 nm Ag. The Ag has a RMS roughness of 1.98 nm, which is almost 4 times larger than that of the Cu:Ag film (RMS = 0.5 nm). c) The cross-section profiles for Cu:Ag and Ag films as deposited on the bare Si wafer (RMS = 0.3 nm).

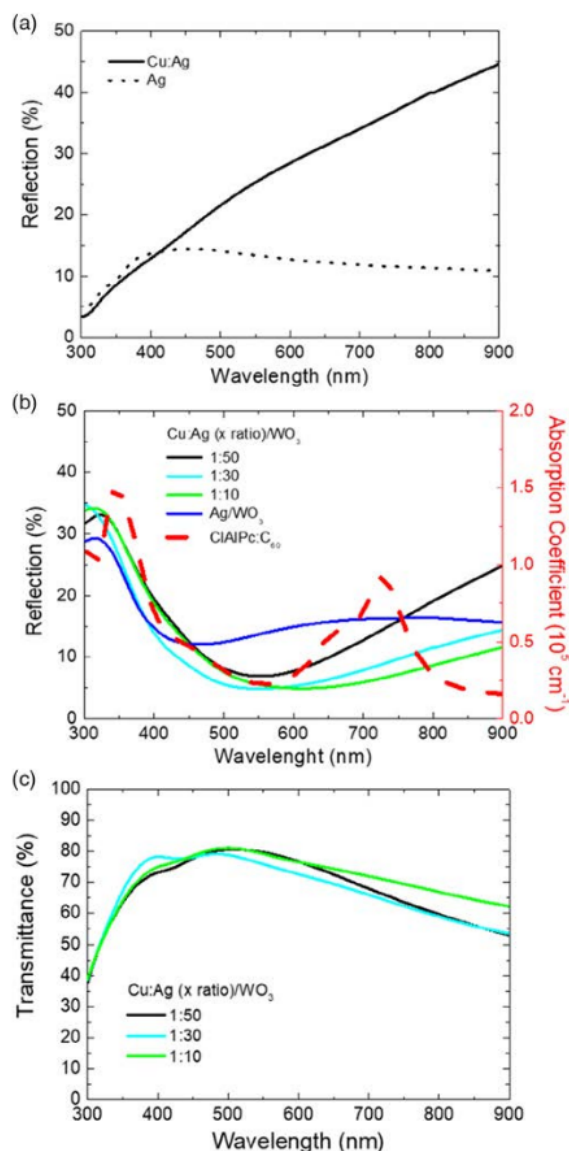


Figure 2. The optical property of ultrathin electrodes and the absorption coefficient of thin films on the bare glass. The value of reflection of a) Cu:Ag (1:50; 8 nm) and Ag (8 nm) and b) Cu:Ag (8 nm; mixing ratio of 1:50, 1:30, and 1:10)/WO₃ (30 nm) and Ag (8 nm)/WO₃ (30 nm). Note that the right axis is the absorption coefficient of ClAlPc:C₆₀ (1:2; 30 nm). c) The transmittance versus wavelength plot for Cu:Ag/WO₃ thin films on the bare glass. The AVT values were 78.62%, 75.19%, and 78.54% for Cu:Ag using the mixing ratio of 1:50, 1:30, and 1:10.

CRI > 90.^[1–3,48] Accordingly, the wavelength-selective ClAlPc/C₆₀ planar heterojunction TPV was demonstrated in 2011,^[8] where the device showed the PCE of ≈1.3% with AVT of ≈65%. The result illustrated a useful strategy for high-efficiency power-generating TPVs. Until now, such wavelength-selective

TPV's working area has been scaled up to one square foot with different materials of the active layers, such as organic molecules, polymers, nanotubes, and salts.^[1–3] Among the various methods of preparing active layers, vacuum deposition process provides a new approach to improve the performance of the small molecular TPVs because the Pc-based donors, i.e., ZnPc,^[49,50] SnPc,^[51,52] PbPc,^[53,54] etc., combined with C₆₀ as acceptor can absorb the UV and NIR light selectively, resulting in the enhancement of the thin-film transparency in the visible light. However, in our previous work, we have demonstrated a single-layer ClAlPc with a planar cyclic intramolecular donor-acceptor structure that allows the direct generation of the excess photocarriers in the absence of any heterojunction interfaces.^[19] In addition, we also found that ClAlPc blended with C₇₀ as an active layer can achieve dark current density <1 nA cm⁻² and specific detectivity >4 × 10¹³ cm Hz^{1/2} W⁻¹ at 730 nm, which might significantly improve the photoresponse property of the organic detectors.^[21] Moreover, ClAlPc shows a high absorption coefficient to cover the UV/NIR region selectively and possess a low highest occupied molecular orbital level to increase the open-circuit voltage (V_{oc}) >0.7 V for OPVs.^[55] In this article, we propose a new approach that uses bulk heterojunction property (BH) of ClAlPc:C₆₀ as the active layer to modify the absorption profile and optical distribution in the device. Sequentially, such OPV combined with the Cu:Ag/WO₃ electrode can reflect the UV/NIR light to enhance photoconversion without impacting the AVT, resulting in the successful demonstration of an efficient TPV with AVT > 75%.

UV/NIR-harvesting OPVs were prepared with the architecture shown in Figure 3a. All materials, fabrication processes, and measurements are described in the Experimental Section. The neat ClAlPc and C₆₀ films selectively absorb only UV or UV/NIR light (Figure 3b), resulting in a semitransparent film. To optimize the transmission value in the visible light, a simple approach is to evaluate the certain mixing ratio of ClAlPc:C₆₀ active layer. For example, ClAlPc:C₆₀ active layer with the mixing ratio of 1:2 allows the light in the visible photopic range (≈450–650 nm) to pass through more effectively compared with neat ClAlPc or C₆₀ film. Similarly, the active layer with different thickness is supposed to alter the device performance as observed in the changes in the J–V curves (Figure 3c). The detail of the device parameters is shown in Table 1. The reference device with 40 nm active layer exhibits a short-circuit current density (J_{sc}) of 6.45 ± 0.07 mA cm⁻², V_{oc} of 0.83 ± 0.01 V, fill factor (FF) of 43.33 ± 0.9%, and PCE of 2.31 ± 0.04%, which is comparable with previous works on the planar structure with the similar thickness of the active layer.^[8,49,50] The external quantum efficiency (EQE) values of OPVs with ClAlPc:C₆₀ strongly depend on the thickness of the active layer, as shown in Figure 3d. It is obvious that the cavity effect and absorption efficiency determine the photogeneration efficiency of ClAlPc:C₆₀, which mainly influences the V_{oc} and J_{sc} as well as the EQE. For the 10 nm active layer, the J_{sc} shows a significantly lower value of 1.56 mA cm⁻² due to the thinner active layer with weak absorption degrading the device performance. However, the EQE spectrum of the OPV maintains the same profile with the increase in the thickness of the active layer, i.e., low absorption in the visible photopic range and relatively high selective absorption in the UV/NIR region. Note that the internal quantum

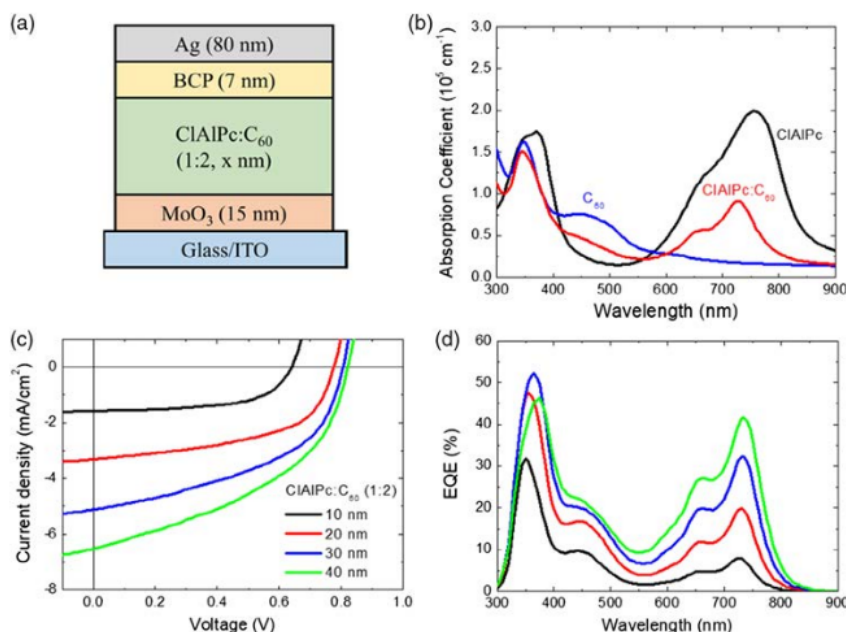


Figure 3. a) Schematic of the CIAIPc:C₆₀ OPV (opaque device). b) The absorption coefficient of CIAIPc, C₆₀, and CIAIPc:C₆₀ (1:2) films. c) Current–voltage (*J*–*V*) and d) EQE curves of CIAIPc:C₆₀ OPVs with different thicknesses, i.e., 10 (black), 20 (red), 30 (blue), and 40 (green) nm for active layer.

Table 1. Device performances of organic photovoltaics based on CIAIPc:C₆₀ (1:2) with different thicknesses of active layer (the values of the standard deviation for each parameter are calculated based on measurement of ten devices).

Thickness [nm]	<i>V</i> _{OC} [V]	<i>J</i> _{SC} [mA cm ⁻²]	FF [%]	PCE [%]	Int. <i>J</i> _{SC} [mA cm ⁻²]	<i>R</i> _{SH} [kΩ cm ²]	<i>R</i> _S [Ω cm ²]
10	0.64 ± 0.00	1.56 ± 0.02	58.39 ± 1.04	0.58 ± 0.01	1.45	4.25 ± 0.81	4.33 ± 0.45
20	0.78 ± 0.01	3.37 ± 0.06	51.00 ± 1.79	1.33 ± 0.05	3.14	1.15 ± 0.12	4.50 ± 0.50
30	0.81 ± 0.01	5.05 ± 0.05	46.26 ± 1.05	1.90 ± 0.06	4.74	0.56 ± 0.03	4.61 ± 0.49
40	0.83 ± 0.01	6.45 ± 0.07	43.33 ± 0.90	2.31 ± 0.04	6.00	0.40 ± 0.03	5.17 ± 1.14

efficiency (IQE) spectra also show similar behavior (Figure S3, Supporting Information), although the active layer's thickness was changed from 10 to 40 nm. Thus, from the IQE/EQE results, the ultrathin active layer of CIAIPc:C₆₀ can convert the photons in the UV/NIR region to charge carriers instantaneously. This could be attributed to the high absorption coefficient of CIAIPc:C₆₀ ($\approx 1 \times 10^5 \text{ cm}^{-1}$) at 375 and 700 nm, suggesting an excellent selective absorption property of our proposed active layer towards the enhancement of the device performance. Therefore, different mixing ratios of CIAIPc:C₆₀ could modify the EQE profile of an OPV, as shown in Figure S4, Supporting Information, which might further lead to more efficient light harvesting in the UV/NIR region.

In this work, we fabricated the TPV with the structure (Figure 4a) as follows: ITO (150 nm)/MoO₃ (15 nm)/CIAIPc:C₆₀ (1:2; 30 nm)/BCP (7 nm)/Cu:Ag (1:50; 8 nm)/WO₃ (30 nm). To investigate the device performance systematically, the transmission (*T*), reflection (*R*), and EQE spectra of the TPV were measured (Figure 4b). Regarding the concept of photon balance, the sum of *T*, *R*, and EQE should be less than unity in every

wavelength to avoid any overestimated value for device efficiency.^[13–16] The proposed wavelength-selective TPV developed in this work exhibits a maximum AVT of approximately 77.45%, which is the highest value compared with the previous work in the TPVs,^[1–3] not segmented PVs,^[56] or transparent luminescent solar concentrators.^[17,18] The TPV devices' surface morphology with different electrodes were analyzed by AFM measurements (see Figure S5, Supporting Information). It can be observed that the TPV device with Ag/WO₃ electrode is relatively rough (RMS = 2.63 nm) contributed from the obvious aggregation and granular structure. On the contrary, the TPV device with Cu:Ag/WO₃ electrode shows a flat surface with relatively smooth profile (RMS = 1.91 nm). In addition, the average value of *T* + *R* + EQE is even greater than 85% in the visible photopic range. Notably, compared with other reference light sources, the AM1.5G solar spectrum can more directly evaluate the performance and aesthetic characteristics of TPV devices. Therefore, the AM1.5G solar spectrum was selected as the benchmark for the characterization of TPV devices in this study.^[57] As the TPV consists of both the selective UV/NIR

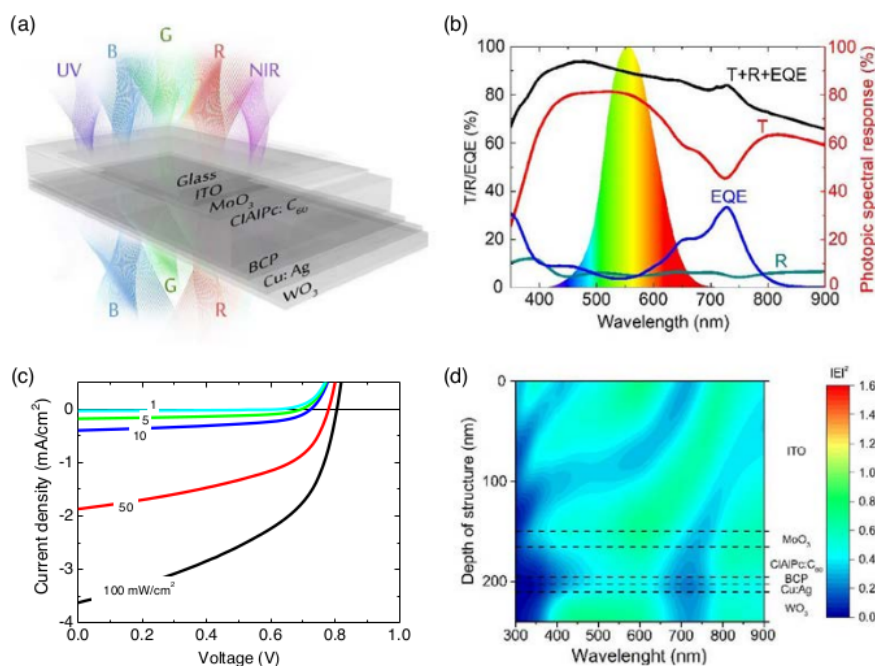


Figure 4. a) The device architecture of proposed TPV. b) The device results, i.e., transmission (T), reflection (R), and EQE for TPV. c) Light intensity-dependent J - V characteristics, and d) optical field distribution of the proposed TPV.

Table 2. Device performances of the proposed TPV based on ClAlPc:C₆₀ (1:2) active layer with different light intensities (the values of the standard deviation for each parameter are calculated based on the measurement of ten devices).

Light intensity [mW cm^{-2}]	V_{oc} [V]	J_{sc} [mA cm^{-2}]	FF [%]	PCE [%]	R_{SH} [$\text{k}\Omega \text{cm}^2$]	R_s [Ωcm^2]
100 (1 sun)	0.80 ± 0.01	3.62 ± 0.01	46.03 ± 0.05	1.34 ± 0.01	0.65 ± 0.01	48.84 ± 1.72
50 (0.5 sun)	0.78 ± 0.01	1.87 ± 0.01	47.39 ± 0.21	1.35 ± 0.02	1.28 ± 0.04	79.63 ± 4.41
10 (0.1 sun)	0.72 ± 0.01	0.40 ± 0.005	49.01 ± 1.44	1.33 ± 0.06	5.70 ± 0.21	342.26 ± 22.30
5 (0.05 sun)	0.69 ± 0.01	0.18 ± 0.001	48.81 ± 2.79	1.27 ± 0.08	13.48 ± 0.66	810.84 ± 63.75
1 (0.01 sun)	0.60 ± 0.01	0.03 ± 0.0001	44.57 ± 3.02	1.01 ± 0.12	55.68 ± 1.73	5217 ± 289.65

absorber (ClAlPc:C₆₀) and transparent electrode (Cu:Ag/WO₃) to visible lights, the device offers a good CRI [Commission Internationale de l'Éclairage 1931, (CIE)] value of ≈ 91.9 (0.31,0.34) in sunlight (AM 1.5G solar spectrum) and reflection <10% in the wavelength range of 400–800 nm, that the tunable color purity of these TPVs originated from the modified transmitted light suggests aesthetics in the display or lighting applications. To evaluate proposed TPV's device performance, J - V characteristics of TPV under various illuminance intensity of AM1.5G from 0.01 to 1 sun were measured (Figure 4c), and the results are shown in Table 2. As the TPV consists of both the selective UV/NIR absorber (ClAlPc:C₆₀) and transparent electrode (Cu:Ag/WO₃) to visible lights, the device offers a good CRI (CIE) value of ≈ 91.9 (0.31,0.34) in sunlight (AM1.5G solar spectrum) and reflection <10% in the wavelength range of 400–800 nm, that the tunable color purity of these TPVs originated from the modified transmitted light suggests aesthetics in the display or lighting applications. To evaluate proposed TPV's device

performance, J - V characteristics of TPV under various illuminance intensity of AM1.5G from 0.01 to 1 sun were measured (Figure 4c) and the results are shown in Table 2.

Under standard sunlight, the optimal TPV shows the J_{sc} of $3.62 \pm 0.01 \text{ mA cm}^{-2}$, V_{oc} of $0.8 \pm 0.01 \text{ V}$, FF of $46.03 \pm 0.05\%$, and PCE of $1.34 \pm 0.01\%$. Here, we demonstrate an ultrahigh transparent TPV with the average PCE value of $\approx 1.34\%$, which is the first work on TPV using organic UV/NIR absorber to achieve AVT over 75%. Unlike inserting a complex optical outcoupling architecture, the CRI of our TPV is improved by exploiting the intrinsic properties of ClAlPc:C₆₀ active layer, i.e., the high-visible transparency (Figure S6, Supporting Information) and selective UV/NIR absorption (Figure S7, Supporting Information) which is responsible in the improvement of the device performance too. Therefore, it is an important result toward the use of selective organic semiconducting material in the development of the TPV performance. It is worthwhile to mention that the increase in the concentration of C₆₀ in the

active layer of ClAlPc:C₆₀ increases the transmission in the NIR region, resulting in the maximization of photopic vision for humans. Furthermore, we also followed CIE Lab method for the TPV devices' colorimetric characteristics.^[57] The transmission CIE Lab (a*, b*) of TPV devices with different active layer ratios are 1:2 (-7.88, -1.99), 1:4 (-4.69, 1.30), 1:6 (-3.05, 1.66), and 1:8 (-1.79, 2.69), respectively (see Table S1, Supporting Information). As the C₆₀ concentration increases, both a* and b* move toward positive values, which corresponds to a significant redshift in the transmission spectrum (\approx 580–700 nm). On the other hand, the reflection spectra with different active layer ratios of TPV devices are shown in Figure S8a, Supporting Information. The reflection CIE Lab (a*, b*) of TPV devices with different active layer ratios are 1:2 (-0.14, 0.75), 1:4 (-6.33, -0.43), 1:6 (-8.73, 0.69), and 1:8 (-11.21, 1.62), respectively. On contrary to the transmission spectrum, as the C₆₀ concentration increases, the reflection intensity for the green to yellow range (about 500–570 nm) increases. Simultaneously, it may induce the decrease in the reflection intensity in the red region. As a consequence, a* moves to negative (green) and b* moves to positive (yellow). The transmission and reflection CIE Lab coordinates of the TPV device are shown in Figure S9, Supporting Information. In addition, the acceptable (a*, b*) ranges for the color of architectural glass products in the market are $-5 < a^* < 1$ and $-5 < b^* < 5$, which highlights in the legend for the green dashed box.^[57] Therefore, ClAlPc:C₆₀ with the mixing ratio of 1:8 offers the AVT of 78.11% and CRI of 95.2 (Figure S10, Supporting Information), where the transparency is much similar to standard ITO glass (CRI \approx 95.7) in an outdoor environment (Figure S11, Supporting Information). Most importantly, this TPV still maintains the PCE of \approx 1.12% (Table S1 and Figure S12, Supporting Information), which is two times higher than that of transparent halide perovskite with high CRI.^[13,14] In addition, the Cu:Ag/WO₃ transparent electrode could act as UV/NIR reflection mirror, whereas its optical capping effect can effectively tune the optical behavior for optimizing the TPV's total transmission value. Figure 4d shows the optical field distribution of the proposed TPV, which is consistent with the reflection and transmission data from thin-film measurements (Figure 4b). Accordingly, we would like to use the parameters of the AVT, PCE, and light utilization efficiency (LUE = PCE \times AVT), as shown in Figure 5, to directly evaluate our TPV devices' performance and compare with the TPV devices proposed by other groups.^[8,9,13,14,16,58–72] As the AVT of our proposed TPV device is approaching >75%, the amount of photons absorbed by the active layer is insufficient, resulting in the poor PCE and LUE values. However, compared with other groups' results, our TPV device still shows the highest AVT while maintaining the PCE at 1.34% and the LUE at 1.03.

2.3. Battery Charging Under Simulated AM1.5G and Low Irradiation

In the previous work, we have demonstrated that the vacuum-deposited OPV can exhibit a PCE close to 16% under a TLD-840 fluorescent lamp (800 lux; 0.232 mW cm⁻²),^[73] which might indicate that new energy-harvesting technology can convert the environmental or sunlight energy efficiently to

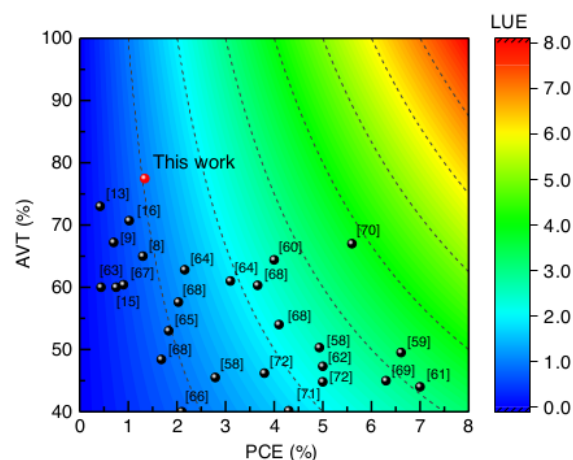


Figure 5. The recent reports (AVT vs PCE vs LUE plot) on the thin-film type TPVs with a UV or UV/NIR-selective mode.^[8,9,13,15,16,58–72] Note that the proposed ClAlPc:C₆₀ TPV with AVT of 77.45% and PCE of 1.34% has been demonstrated in this work.

drive low-power-consumption electronics.^[74] Several materials and systems, such as OPVs,^[53,54,75] dye-sensitized solar cells,^[76] polymer solar cells,^[77–79] and perovskite PVs^[80,81] have been used to achieve high-efficiency self-sustainable power in the past 3 years.^[82] Here, we propose that the TPV module developed in this work can directly charge a homemade LiFePO₄ (LFP) battery (CR2032 coin cell; Figure S13, Supporting Information) with a capacity of 0.58 mAh under the sunlight. Note that the active area is 1.5 cm² for the module (0.04 cm² for a single device), showing PCE of \approx 1.3% (Figure 6a). The TPV module's performance under different sunlight intensities is shown in Table 3 and Figure 6b. For the homemade battery, the operation voltage for charging was set to around 3.4 V, i.e., the module could fully charge the battery if its V_{oc} exceeds 3.5 V. The operating time strongly depends on the charging efficiency.^[83] Our transparent TPV module exhibits the V_{oc} (V_{max}) of 4.27 (2.8) V and I_{sc} (I_{max}) of 1.08 (0.75) mA under illumination intensity of 100 mW cm⁻² (\approx 1 sun), and charges the battery fully in just over 57 min. The total charging time increases approximately linearly with light intensity as expected (Figure 6c). Although the charging time is still too long for a particular application, the transparent module can probably be integrated with a microbattery or small-sized storage unit to deliver self-sustainable power by converting the energy from the sunlight. It should be noted that the prolonged charging time is due to the smaller active area of our module (1.5 cm²), which limits the charging efficiency or increases the operating time. However, this transparent TPV module on a cover glass is able to provide self-sustainable power for wearable electronics. For example, even under as low as 5 mW cm⁻² (\approx 0.05 sun) incident intensity, the TPV module is able to produce sufficient power with V_{max} of 2.3 V and I_{max} of 34.2 μ A to drive the exciplex OLEDs emitting the luminance >180 cd m⁻² (Figure 6d and Figure S14, Supporting Information), which is promising in extending the operation time for augmented reality glasses or other low-power-consumption electronics.

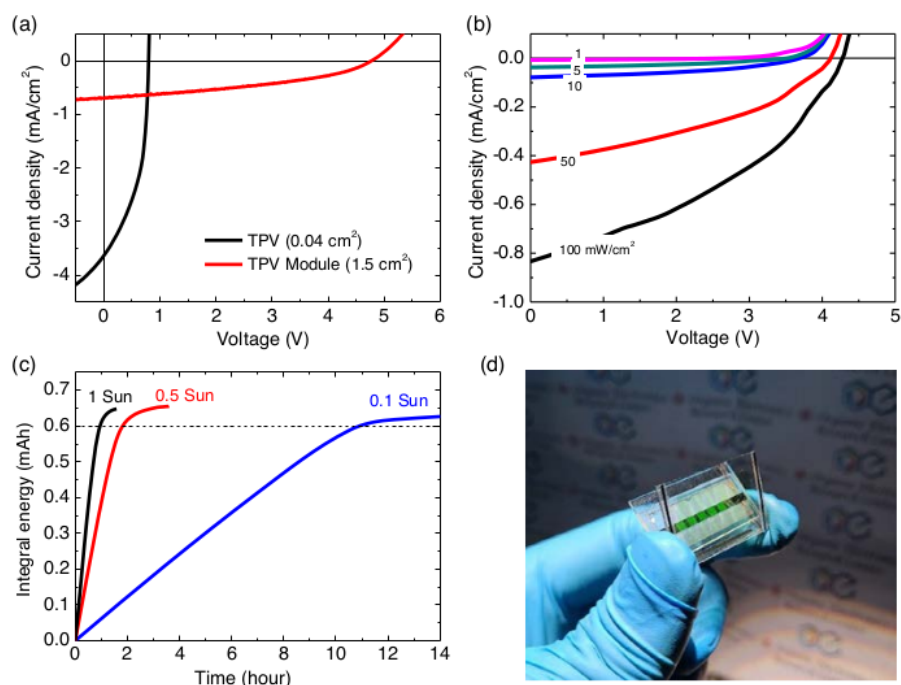


Figure 6. The *JV* characteristics under the a) 1 sun for the single TPV and TPV module and b) different sunlight intensities for the TPV module. c) The plot of the charging time versus time for the TPV module under different sunlight intensities. Note that the active area of our proposed module is 1.5 cm². d) The demo picture shows that the TPV module can convert the sunlight with 0.05 sun (5 mW cm⁻²) to drive an exciplex OLEDs to emit 180 cd m⁻².

Table 3. Device performances of the TPV module with different light intensities (the values of the standard deviation for each parameter are calculated based on the measurement of six devices).

Light intensity [mW cm ⁻²]	V _{OC} [V]	J _{SC} [mA cm ⁻²]	FF [%]	PCE [%]	V _{max} [V]	I _{max} [mA]
100 (1 sun)	4.70 ± 0.09	1.13 ± 0.04	42.30 ± 19.60	1.30 ± 0.07	3.11 ± 0.54	0.59 ± 0.18
50 (0.5 sun)	4.45 ± 0.11	0.50 ± 0.15	43.12 ± 17.52	1.26 ± 0.26	2.98 ± 0.31	0.29 ± 0.07
10 (0.1 sun)	3.83 ± 0.21	0.12 ± 0.004	36.60 ± 1.53	1.17 ± 0.11	2.40 ± 0.20	0.07 ± 0.003
5 (0.05 sun)	3.43 ± 0.31	0.06 ± 0.002	35.83 ± 2.41	1.04 ± 0.16	2.28 ± 0.20	0.034 ± 0.001
1 (0.01 sun)	2.13 ± 0.57	0.01 ± 0.0003	33.90 ± 1.88	0.63 ± 0.19	1.25 ± 0.18	0.01 ± 0.0003

3. Conclusion

In summary, we have demonstrated a TPV based on selective UV/NIR ClAlPc:C₆₀ absorber with a record average visible transmission of up to 77%. With the transparent electrode of Cu:Ag/WO₃, the TPV shows the PCE of 1.34% and CRI of 91.9, as well as its *T* + *R* + EQE is (the average value) over 85% in the wavelength range of 450–650 nm. Compared with the research results of organic TPVs by other groups, our proposed TPV shows the highest AVT. Notably, the ClAlPc:C₆₀ active layer with the mixing ratio of 1:8 could further modify the CRI from 91.9 to 95.2, which is similar to bare ITO glass. As a result, the TPV module is also capable to fully charge a 0.58 mAh battery within 1 h when the device is exposed under

1 sun illuminance. In addition, such invisible solar technology could be used to drive an exciplex OLED to emit the brightness of ≈180 cd m⁻² under the low illuminance of ≈5 mW cm⁻². This work represents a significant step forward in the development of the TPV integrated to a display unit serving as a transparent sustainable solar power.

4. Experimental Section

TPV and Module Fabrications: All organic and inorganic materials were purchased from Merck KGaA (Sigma-Aldrich), including the molybdenum oxide (MoO₃), chloroaluminum phthalocyanine (ClAlPc), fullerene (C₆₀), bathocuproine (BCP), copper (Cu), silver (Ag), and tungsten trioxide (WO₃). Among these materials, only organic material of ClAlPc had been

sublimated twice using a homemade graded purification system with a high vacuum level of $\approx 2 \times 10^{-2}$ torr before the device fabrication. After this, the ITO substrates ($15 \Omega \text{sq}^{-1}$; Lumtec) followed the standard clean procedure that carried out in the ultrasonic vibration tank for soaked in different solutions, i.e., deionized water, acetone, isopropyl, and dried by nitrogen gas. For TPV device preparation, the device configuration of the TPV with the structure of ITO/MoO₃ (15 nm)/ClAlPc:C₆₀ (1:2; 30 nm)/BCP (7 nm)/Cu:Ag (1:50; 8 nm)/WO₃ (30 nm) and the active layer of 0.04 cm² were fabricated in the thermal evaporator under 5×10^{-6} torr. Note that the active area of the device was defined by the overlapping area of the anode and cathode electrodes. The deposition of each material was set at a constant rate of $\approx 0.5 \text{ \AA s}^{-1}$. Finally, the sample was encapsulated by the bare glass and sealed with a UV-curable adhesive, which was carried out in the N₂ glovebox without oxygen and moisture (<0.1 ppm). On the other hand, six OPV cells were connected in series (0.25 cm² per cell) to fabricate the TPV module. To encapsulate the TPV module, the method of chemical vapor deposition was used to deposit a 1 μm transparent parylene (Transmission value >95% in the visible light) thin film on the TPV module, which can well protect the device to avoid the environmental degradation during the electrical and optical measurements.

Photophysical and Surface Morphology Analysis: All thin films were deposited on the bare glass. Among these, quartz glass was used only in the measurement of the absorption coefficient. The transmission, reflection, and absorption measurements were carried out using a UV-vis spectrophotometer (Jasco, V-770) in ambient conditions. The morphology of the thin films deposited on the silicon substrate were measured by an atomic force microscope (Bruker, INNOVA) with the noncontact mode to use the silicon tip (FESPA-V2).

TPV and Module Measurements: The electrical characteristics of the TPV devices with covered 4 mm² shadow mask were measured by a source meter (Keithley 2400) under a 3A xenon lamp solar simulator with the intensity of 100 mW cm⁻² (Enli Tech, SS-X100R). For the PV measurements, the method was calibrated by ISO/IEC 17025 certified lab, which traced to NREL. The spectral mismatch factor was 1.005 as according to IEC-60904-7 and NREL testing protocol. The EQE spectrum was measured with a QE-R Solar Cell Spectral Response Measurement System (Enli Technology Co., Ltd., Taiwan). In addition, the monochromatic light was chopped at 200 Hz calibrated by two certified photodetectors (Si and Ge) for the QE-R system. The calibration and testing procedures were followed IEC 60904-8: 2014 and ASTM E 1201 standards of PV spectral response testing. For the TPV module measurement, the measuring procedure of electrical characteristics was followed by the standard TPV as described earlier. To evaluate the charging efficiency, the capacity value of 0.6 mAh was defined to the threshold level, which means the battery with full energy. Accordingly, the charging current of the TPV module was recorded by Keithley 2400 with the Labview program for different sunlight intensities.

The Internal Quantum Efficiency of Photovoltaics Measurement: The IQE spectra of the devices were plotted based on the measurement of EQE spectra and the corresponding absorption efficiency $A(\lambda)$. The $A(\lambda)$ values were calculated out from the equation $A(\lambda) = 100\% - T(\lambda) - R(\lambda)$, where $T(\lambda)$ and $R(\lambda)$ are the transmission and the reflection efficiencies, respectively. Note that the values of $T(\lambda)$ and $R(\lambda)$ of the device were measured by a spectrophotometer equipped with an integration sphere (V-700, Jasco). Finally, the IQE values were estimated by dividing the EQE spectrum with $A(\lambda)$ values in each wavelength.^[84]

OLED Preparation and Characterizations: All OLED materials such as Hexaazatriphenylhexacarbonitrile (HATCN), 1,1-bis[(di-4-tolylamino)phenyl]cyclohexane (TAPC), 4,6-bis(3,5-di(pyridin-3-yl)phenyl)-2-methylpyrimidine (B3PYMPM), bis[2-(2-pyridinyl-N)phenyl-C](acetylacetonato)iridium(III) (Ir(ppy)₂acac) were purchased from Shine Materials Technology Co., Ltd. The device structure was sputtered ITO (80 nm)/HATCN (10 nm)/TAPC (20 nm)/TcTa (15 nm)/B3PYMPM (1:1; 30 nm): 8 wt% Ir(ppy)₂(acac)/B3PYMPM (50 nm)/LiF (1 nm)/Al (100 nm), which completely followed the previous method to prepare the efficient exciplex OLED with EQE of $\approx 33.2\%$.^[85] The luminance-current-voltage ($L-I-V$) characteristics of exciplex OLEDs were measured

using the LQ-100X system from Enli technology, which calibrated with a PR655 spectrophotometer (Photo Research, USA).

Optical Simulation: Transfer matrix method (TMM)^[86] was used to calculate the electric field distribution in the TPV devices. For the optical simulation, we have used the standard TPV structure that follows: glass/ITO (150 nm)/MoO₃ (15 nm)/ClAlPc:C₆₀ (1:2, 30 nm)/BCP (7 nm)/Cu:Ag (1:50, 8 nm)/WO₃ (30 nm). To input the intrinsic parameters of all layers in the optical model, the wavelength-dependent refractive index (n) and extinction coefficient (k) of each thin film were measured by an ellipsometer (SE-950, Radiation Technology Co., Ltd.). All thin films were deposited using the thermal evaporator on the Si wafer with a thickness of ≈ 100 nm.

LFP/Li Cells Preparation: LFP/Li cells (CR2032-type coin cells) were composed of a homemade LFP/C composite cathode,^[87] a commercial polyethylene microporous separator (diameter: ≈ 1.8 cm, thickness: ≈ 16 μm , Asahi Kasei Corp., Japan), and a lithium metallic foil (diameter: ≈ 1.6 cm, ≈ 450 μm in thickness) as the anode, followed by activation with the liquid electrolyte of 1 M lithium hexafluorophosphate (LiPF₆) dissolved in ethylene carbonate (EC)/diethyl carbonate (DEC) (EC:DEC = 1/1, v/v). All cell assemblies were carried out in an argon-filled glove box (TTS100-1, MBRAUN UniLab-B, Germany; H₂O and O₂ < 0.5 ppm). Before testing, the assembled cells with a capacity of 0.58 mAh were activated galvanostatically at a constant current rate of 0.05C (0.032 mA) between 3.0 and 4.0 V (vs Li/Li⁺) at ambient temperature using a battery cyler (BCS-805, BioLogic, France).

2 Supporting Information

Supporting Information is available from the Wiley Online Library or from the author.

Acknowledgements

The authors acknowledge financial support from the Ministry of Science and Technology (Grant Nos. MOST 107-2221-E-131-029-MY2, 108-2221-E-131-027-MY2, 108-2221-E-011-151, 108-3116-F-131-001-CC1, 109-3116-F-131-001-CC1, 109-2221-E-131-002, 109-2221-E-011-156, and 109-2223-E-131-001-MY3) and industry project from the Central Taiwan Science Park (108RB04). The corresponding author (S.-W. Liu) is grateful to Mr. H.-H. Wu, Syskey Technology Co., Ltd (Taiwan), for his assistance in designing the fabrication system.

Conflict of Interest

The authors declare no conflict of interest.

Keywords

battery charging, highly transparent photovoltaics, invisible solar technologies, sustainable solar power, transparent electrodes

Received: September 10, 2020

Revised: December 2, 2020

Published online: December 15, 2020

- [1] C. J. Traverse, R. Pandey, M. C. Barr, R. R. Lunt, *Nat. Energy* **2017**, *2*, 849.
- [2] C. J. M. Emmott, J. A. Röhr, M. Campoy-Quiles, T. Kirchartz, A. Urbina, N. J. Ekins-Daukes, J. Nelson, *Energy Environ. Sci.* **2015**, *8*, 1317.
- [3] S.-Y. Cheng, P. Cheng, G. Li, Y. Yang, *Joule* **2018**, *2*, 1039.

- [4] Y. Li, J.-D. Lin, X. Che, Y. Qu, F. Liu, L.-S. Liao, S. R. Forrest, *J. Am. Chem. Soc.* **2017**, 139, 17114.
- [5] Y. Cui, C. Yang, H. Yao, J. Zhu, Y. Wang, Y. Wang, G. Jia, F. Gao, J. Hou, *Adv. Mater.* **2017**, 29, 1703080.
- [6] R. Betancur, P. Romero-Gomez, A. Martinez-Otero, X. Elias, M. Maymó, J. Martorell, *Nat. Photon.* **2013**, 7, 995.
- [7] W. Wang, C. Yan, T.-K. Lau, J. Wang, K. Liu, Y. Fan, X. Lu, X. Zhan, *Adv. Mater.* **2017**, 29, 1701308.
- [8] R. R. Lunt, V. Bulovic, *Appl. Phys. Lett.* **2011**, 98, 113305.
- [9] H. Zhang, G. Wicht, C. Getener, M. Nagel, F. Nüesch, Y. Romanyuk, J.-N. Tisserant, R. Hany, *Sol. Energy Mater. Sol.* **2013**, 118, 157.
- [10] E. Berner, T. Jäger, T. Lanz, F. Nüesch, J.-N. Tisserant, G. Wicht, H. Zhang, R. Hany, *Appl. Phys. Lett.* **2013**, 102, 183903.
- [11] K. Kakiage, Y. Aoyama, T. Yano, K. Oya, J. Fujisawa, M. Hanaya, *Chem. Commun.* **2015**, 51, 15894.
- [12] S. Yoon, S. Tak, J. Kim, Y. Jun, K. Kang, J. Park, *Build. Environ.* **2011**, 46, 1899.
- [13] D. Liu, C. Yang, R. R. Lunt, *Joule* **2018**, 2, 1827.
- [14] C. Hanmandlu, C.-Y. Chen, K. M. Boopathi, H.-W. Lin, C.-S. Lai, C.-W. Chu, *ACS Appl. Mater. Interfaces* **2017**, 9, 32635.
- [15] K. M. Boopathi, C. Hanmandlu, A. Singh, Y.-F. Chen, C.-S. Lai, C.-W. Chu, *ACS Appl. Energy Mater.* **2018**, 1, 632.
- [16] D. Liu, C. Yang, P. Chen, M. Bates, S. Han, P. Askeland, R. R. Lunt, *ACS Appl. Energy Mater.* **2019**, 2, 3972.
- [17] Y. Zhao, G. A. Meek, B. G. Levine, R. R. Lunt, *Adv. Opt. Mater.* **2014**, 2, 606.
- [18] C. Yang, M. Moemeni, M. Baes, W. Sheng, B. Borhan, R. R. Lunt, *Adv. Opt. Mater.* **2020**, 8, 1901536.
- [19] M. Wang, Y.-Z. Li, H.-C. Chen, C.-W. Liu, Y.-S. Chen, Y.-C. Lo, C.-T. Tsao, Y.-C. Huang, S.-W. Liu, K.-T. Wong, B. Hu, *Mater. Horiz.* **2020**, 7, 1171.
- [20] Y. Zou, Z. Deng, W. J. Potscavage, M. Hirade, Y. Zheng, C. Adachi, *Appl. Phys. Lett.* **2012**, 100, 243302.
- [21] C.-C. Lee, R. Estrada, Y.-Z. Li, S. Biring, N. R. A. Amin, M.-Z. Li, S.-W. Liu, K.-T. Wong, *Adv. Opt. Mater.* **2020**, 8, 2000519.
- [22] C.-H. Yuan, C.-C. Lee, C.-F. Liu, Y.-H. Lin, W.-C. Su, S.-Y. Lin, K.-T. Chen, Y.-D. Li, W.-C. Chang, Y.-Z. Li, T.-H. Su, Y.-H. Liu, S.-W. Liu, *Sci. Report.* **2016**, 6, 32324.
- [23] S.-M. Lee, J.-H. Kwon, K.-C. Choi, *IEEE Trans. Electron Devices* **2017**, 64, 1922.
- [24] J. H. Koo, D. C. Kim, H. J. Shim, T.-H. Kim, D.-H. Kim, *Adv. Funct. Mater.* **2018**, 28, 1801834.
- [25] W.-L. Tsai, C.-Y. Chen, Y.-T. Wen, L. Yang, Y.-L. Cheng, H.-W. Lin, *Adv. Mater.* **2019**, 13, 1900231.
- [26] M. Kaltenbrunner, T. Sekitani, J. Reeder, T. Yokota, K. Kuribara, T. Tokuhara, M. Drack, R. Schwödiauer, I. Graz, S. Bauer-Gogonea, S. Bauer, T. Someya, *Nature* **2013**, 499, 458.
- [27] T. Someya, Z. Bao, G. G. Malliaras, *Nature* **2016**, 540, 379.
- [28] Y. Liu, P. Cheng, T. Li, R. Wang, Y. Li, S. Y. Chang, Y. Zhu, H.-W. Cheng, K.-H. Wei, X. Zhan, B. Sun, Y. Yang, *ACS Nano* **2019**, 13, 1071.
- [29] X. Ren, X. Li, W. C. H. Choy, *Nano Energy* **2015**, 17, 187.
- [30] H. M. Stec, R. A. Hatton, *ACS Appl. Mater. Interfaces* **2012**, 4, 6013.
- [31] Y.-G. Bi, Y.-F. Liu, X.-L. Zhang, D. Yin, W.-Q. Wang, J. Feng, H.-B. Sun, *Adv. Opt. Mater.* **2019**, 7, 1800778.
- [32] Y. Liu, T. Ding, X. Chen, F. Bai, A. Genco, H. Wang, C. Chen, P. Chen, M. Mazzeo, Y. Zhang, Y. Duan, *Appl. Opt. Mater.* **2020**, 8, 2000206.
- [33] S.-W. Liu, T.-H. Su, P.-C. Chang, T.-H. Yeh, Y.-Z. Li, L.-J. Huang, Y.-H. Chen, C.-F. Lin, *Org. Electron.* **2016**, 31, 240.
- [34] N. Formica, P. Mantilla-Perez, D. S. Ghosh, D. Janner, T. L. Chen, M. Huang, S. Gamer, J. Martorell, V. Pruneri, *ACS Appl. Mater. Interfaces* **2015**, 7, 4541.
- [35] Z. C. Xue, X. Y. Liu, N. Zhang, H. Chen, X. M. Zheng, H. Y. Wang, X. Y. Guo, *ACS Appl. Mater. Interfaces* **2014**, 6, 16403.
- [36] S.-W. Liu, T.-H. Su, Y.-Z. Li, *Org. Electron.* **2014**, 15, 1990.
- [37] T.-H. Yeh, C.-C. Lee, C.-J. Shih, G. Kumar, S. Biring, S.-W. Liu, *Org. Electron.* **2018**, 59, 266.
- [38] K. H. Choi, J. Y. Kim, Y. S. Lee, H. J. Kim, *Thin Solid Films* **1999**, 341, 152.
- [39] D. R. Sahu, S.-Y. Lin, J.-L. Huang, *Sol. Energy Mater. Sol. Cells* **2007**, 91, 851.
- [40] G. Kumar, Y.-D. Li, S. Biring, Y.-N. Lin, S.-W. Liu, C.-H. Chang, *Org. Electron.* **2017**, 42, 52.
- [41] Y. Li, C. Ji, Y. Qu, X. Huang, S. Hou, C.-Z. Li, L.-S. Liao, L. J. Guo, S. R. Forrest, *Adv. Mater.* **2019**, 31, 1903173.
- [42] C. T. Campbell, *Surf. Sci. Rep.* **1997**, 27, 1.
- [43] A. Anders, E. Byon, D.-H. Kim, K. Fukuda, S. H. N. Lim, *Solid State Commun.* **2006**, 140, 225.
- [44] H. Liu, B. Wang, E. S. P. Leong, P. Yang, Y. Zong, G. Y. Si, J. H. Teng, S. A. Maier, *ACS Nano* **2010**, 4, 3139.
- [45] J. Bulíř, M. Novotný, A. Lunnykova, J. Lančok, *J. Nanophotonics* **2011**, 5, 051511.
- [46] N. P. Sergeant, A. Hadipour, B. Niesen, D. Cheyns, P. Heremans, P. Peumans, B. P. Rand, *Adv. Mater.* **2012**, 24, 728.
- [47] H. W. Edwards, R. P. Petersen, *Phys. Rev.* **1936**, 50, 871.
- [48] R. R. Lunt, *Appl. Phys. Lett.* **2012**, 101, 043902.
- [49] W. Zeng, K. S. Yong, Z. M. Kam, F. Zhu, Y. Li, *Appl. Phys. Lett.* **2010**, 97, 133304.
- [50] F. T. Reis, D. Mencaraglia, S. O. Saad, I. Séguy, M. Oukachmih, P. Jolinat, P. Destruel, *Syn. Met.* **2003**, 138, 33.
- [51] B. P. Rand, J. Xue, F. Yan, S. R. Forrest, *Appl. Phys. Lett.* **2005**, 87, 233508.
- [52] D. Y. Kim, G. Sarasqueta, F. So, *Sol. En. Mater. Sol. Cell.* **2009**, 93, 1452.
- [53] H.-S. Shim, H. J. Kim, J. W. Kim, S.-Y. Kim, W.-I. Jeong, T.-M. Kim, J.-J. Kim, *J. Mater. Chem.* **2012**, 22, 9077.
- [54] M. Hiramoto, K. Kitada, T. Kaji, *Appl. Phys. Lett.* **2011**, 98, 023302.
- [55] R. F. Bailey-Salzman, B. P. Rand, S. R. Forrest, *Appl. Phys. Lett.* **2007**, 91, 013508.
- [56] J. Yoon, A. J. Baca, S.-I. Park, P. Elvikis, J. B. Geddes III, L. Li, R. H. Kim, J. Xiao, S. Wang, T.-H. Kim, M. J. Mettala, B. Y. Ahn, E. B. Duoss, J. A. Lewis, R. G. Nuzzo, P. M. Ferreira, Y. Huang, A. Rockett, J. A. Rogers, *Nat. Mater.* **2008**, 7, 907.
- [57] C. Yang, D. Liu, M. Bates, M. C. Barr, R. R. Lunt, *Joule*, **2019**, 3, 1.
- [58] G. Ji, Y. Wang, Q. Luo, K. Han, M. Xie, L. Zhang, N. Wu, J. Lin, S. Xiao, Y.-Q. Li, L.-Q. Luo, C.-Q. Ma, *ACS Appl. Mater. Interfaces* **2018**, 10, 943.
- [59] X. Du, X. Li, H. Lin, L. Zhou, C. Zheng, S. Tao, *J. Mater. Chem. A* **2019**, 7, 7437.
- [60] C.-C. Chen, L. Dou, R. Zhu, C.-H. Chung, T.-B. Song, Y. B. Zheng, S. Hawks, G. Li, P. S. Weiss, Y. Yang, *ACS Nano*, **2012**, 6, 7185.
- [61] X. Li, H. Meng, F. Shen, D. Su, S. Huo, J. Shan, J. Huang, C. Zhan, *Dyes Pigment.* **2019**, 166, 196.
- [62] C.-Y. Chang, L. Zuo, H.-L. Yip, Y. Li, C.-Z. Li, C.-S. Hsu, Y.-J. Cheng, H. Chen, A. K.-Y. Jen, *Adv. Funct. Mater.* **2013**, 23, 5084.
- [63] Y. Peng, L. Zhan, N. Cheng, T. L. Andrew, *Energies* **2017**, 10, 707.
- [64] Y. Song, S. Chang, S. Gradecak, J. Kong, *Adv. Energy Mater.* **2016**, 6, 1600847.
- [65] W. J. D. Silva, H. P. Kim, A. R. B. M. Yusoff, J. Jang, *Nanoscale* **2013**, 5, 9324.
- [66] J. Meiss, K. Leo, M. K. Riede, C. Uhrich, W.-M. Gnehr, S. Sonntag, M. Pfeiffer, *Appl. Phys. Lett.* **2009**, 95, 213306.
- [67] J. Suddard-Bangsund, C. J. Traverse, M. Young, T. J. Patrick, Y. Zhao, R. R. Lunt, *Adv. Energy Mater.* **2016**, 6, 1501659.
- [68] K. Zhang, C. Qin, X. Yang, A. Islam, S. Zhang, H. Chen, Liyuan Han, *Adv. Energy Mater.* **2014**, 4, 1301966.
- [69] F. Liu, Z. Zhou, C. Zhang, J. Zhang, Q. Hu, T. Vergote, F. Liu, T. P. Russell, X. Zhu, *Adv. Mater.* **2017**, 29, 1606574.

- [70] M. Zhang, X. Guo, W. Ma, H. Ade, J. Hou, *Adv. Mater.* **2015**, *27*, 4655.
- [71] N. Zhang, G. Chen, Y. Xu, X. Xu, L. Yu, *ACS Appl. Energy Mater.* **2019**, *2*, 6060.
- [72] Y. Xie, L. Huo, B. Fan, H. Fu, Y. Cai, L. Zhang, Z. Li, Y. Wang, W. Ma, Y. Chen, Y. Sun, *Adv. Funct. Mater.* **2018**, *28*, 1800627.
- [73] C.-H. Chen, H.-C. Ting, Y.-Z. Li, Y.-C. Lo, P.-H. Sher, J.-K. Wang, T.-L. Chiu, C.-F. Lin, I.-S. Hsu, J.-H. Lee, S.-W. Liu, K.-T. Wong, *ACS Appl. Mater. Interfaces* **2019**, *11*, 8337.
- [74] Y. Gao, Y. Liu, S. M. Zakeeruddin, A. Hagfeldt, M. Grätzel, *Joule* **2018**, *2*, 1108.
- [75] H. K. H. Lee, J. Wu, J. Barbé, S. M. Jain, S. Wood, E. M. Speller, Z. Li, F. A. Castro, J. R. Durrant, W. C. Tsoi, *J. Mater. Chem. A* **2018**, *6*, 5618.
- [76] Y. S. Tingare, N. S. Vinh, H.-H. Chou, Y.-C. Liu, Y.-S. Long, T.-C. Wu, T.-C. Wei, C.-Y. Yeh, *Adv. Energy Mater.* **2017**, *7*, 1700032.
- [77] C.-Y. Liao, Y. Chen, C.-C. Lee, G. Wang, N.-W. Teng, C.-H. Lee, W.-L. Li, Y.-K. Chen, C.-H. Li, H.-L. Ho, P. H.-S. Tan, B. Wang, Y.-C. Huang, R.-M. Young, M. R. Wasielewski, T. J. Marks, Y.-M. Chang, A. Facchetti, *Joule* **2020**, *4*, 189.
- [78] Y. Chi, Y. Wang, J. Bergqvist, H. Yao, Y. Xu, B. Gao, C. Yang, S. Zhang, O. Inganäs, F. Gao, J. Hou, *Nat. Energy* **2019**, *4*, 768.
- [79] Y.-J. You, C. E. Song, Q. V. Hoang, Y. Kang, J. S. Goo, D.-H. Ko, J.-J. Lee, W. S. Shin, J. W. Shim, *Adv. Funct. Mater.* **2019**, *29*, 1901171.
- [80] C.-Y. Chen, J.-H. Chang, K.-M. Chiang, H.-L. Lin, Y.-S. Hsiao, H.-W. Lin, *Adv. Funct. Mater.* **2015**, *25*, 7064.
- [81] M. Li, C. Zhao, Z.-K. Wang, C.-C. Zhang, H. K. H. Lee, A. Pockett, J. Barbé, C. W. Tsoi, Y.-G. Yang, M. J. Carnie, X. Y. Gao, W.-X. Yang, J. R. Durrant, L.-S. Liao, S. M. Jain, *Adv. Energy Mater.* **2018**, *8*, 1801509.
- [82] A. Venkateswararao, J. K. W. Ho, S. K. So, S.-W. Liu, K.-T. Wong, *Mater. Sci. Eng. R Rep.* **2020**, *139*, 100517.
- [83] P. Sullivan, S. Schumann, R. D. Campo, T. Howells, A. Duraud, M. Shiman, R. A. Hatton, T. S. Jones, *Adv. Energy Mater.* **2013**, *3*, 239.
- [84] C.-F. Lin, S.-W. Liu, C.-C. Lee, T. Sakurai, M. Kubota, W.-C. Su, J.-C. Huang, T.-L. Chiu, H.-C. Han, L.-C. Chen, C.-T. Chen, J.-H. Lee, *Sol. Energy Mater. Sol. Cells* **2015**, *137*, 138.
- [85] C.-C. Lee, C.-J. Shih, G. Kumar, S. Biring, S. Sen, S.-W. Liu, *J. Mater. Chem. C* **2017**, *5*, 12050.
- [86] G. F. Burkhard, E. T. Hoke, M. D. McGehee, *Adv. Mater.* **2010**, *22*, 3293.
- [87] Y.-S. Wu, C.-C. Yang, S.-P. Luo, Y.-L. Chen, C.-N. Wei, S. J. Lue, *Int. J. Hydrog. Energy* **2017**, *42*, 6862.

Vacuum-Deposited Transparent Organic Photovoltaics for Efficiently Harvesting Selective Ultraviolet and Near-Infrared Solar Energy

ORIGINALITY REPORT

3%

SIMILARITY INDEX

2%

INTERNET SOURCES

4%

PUBLICATIONS

1%

STUDENT PAPERS

PRIMARY SOURCES

1

hdl.handle.net

Internet Source

1%

2

Yi - Sheng Chen, Dian Luo, Wei - Chih Wei, Bo - Lin Chen, Tzu - Hung Yeh, Shun - Wei Liu, Ken - Tsung Wong. "New Exciplex - Forming Co - Host System and Thienothiadazole - based Fluorescent Emitter for High - Efficiency and Promising Stability Near - Infrared OLED", *Advanced Optical Materials*, 2021

Publication

1%

3

Yun-Ming Sung, Meng-Zhen Li, Dian Luo, Yan-De Li, Sajal Biring, Yu-Ching Huang, Chun-Kai Wang, Shun-Wei Liu, Ken-Tseng Wong. "A new micro-cavity forming electrode with high thermal stability for semi-transparent colorful organic photovoltaics exceeding 13% power conversion efficiency", *Nano Energy*, 2020

Publication

1%

4

Chi-Feng Lin, Shun-Wei Liu, Chih-Chien Lee, Takeaki Sakurai et al. "A new anodic buffer layer material for non-mixed planar heterojunction chloroboron subphthalocyanine organic photovoltaic achieving 96% internal quantum efficiency", *Solar Energy Materials and Solar Cells*, 2015

Publication

1 %

Exclude quotes Off

Exclude matches < 1%

Exclude bibliography On